RSC Advances

PAPER

View Article Online
View Journal | View Issue

Cite this: *RSC Adv.*, 2018, **8**, 21513

Characterization of palladium species after γ-irradiation of a TBP–alkane–$Pd(NO_3)_2$ system†

Bénédicte Simon,[a] Christine Bouyer,*[a] Stéphanie De Sio,[b] Claude Berthon,[a] Nathalie Boubals,[a] Frédéric Miserque,[c] Emmanuelle Brackx,[a] Nicole Raymond,[a] Alexandre Chagnes[d] and Laurence Berthon[a]

Received 28th March 2018
Accepted 1st June 2018

DOI: 10.1039/c8ra02695e

rsc.li/rsc-advances

The γ-irradiation of a biphasic system composed of tri-*n*-butylphosphate in tetrapropylene hydrogen (TPH) in contact with palladium(II) nitrate in nitric acid aqueous solution led to the formation of two precipitates. A thorough characterization of these solids was performed by means of various analytical techniques including X-Ray Diffraction (XRD), Thermal Gravimetric Analysis coupled with a Differential Scanning Calorimeter (TGA-DSC), X-ray Photoelectron Spectroscopy (XPS), InfraRed (IR), RAMAN and Nuclear Magnetic Resonance (NMR) Spectroscopy, and ElectroSpray Ionization Mass Spectrometry (ESI-MS). Investigations showed that the two precipitates exhibit quite similar structures. They are composed at least of two compounds: palladium cyanide and palladium species containing ammonium, phosphorous or carbonyl groups. Several mechanisms are proposed to explain the formation of $Pd(CN)_2$.

Introduction

In the PUREX process, 30%$_{vol}$ tri-*n*-butylphosphate (TBP) diluted in Tetra Propylene Hydrogen (TPH, a hydrocarbon diluent) is used to extract uranium and plutonium from fission products (ruthenium, molybdenum, cesium, palladium, *etc.*) and minor actinides contained in spent nuclear fuels.[1,2] Due to the biphasic nature of the chemical system and the presence of numerous solutes (nitric acid, uranium, plutonium, fission products…), the solvent is subject to hydrolytic and radiolytic degradation. The resulting damage can modify the solution composition, alter the physico-chemical properties, modify the extraction kinetics, and modify the redox properties of the metallic ions to be extracted.[3] Since the 1950s, many studies have been focused on the investigation of the stability of TBP and diluent under radioactive stress.[3,4] In particular, the influence of the irradiation source (α-irradiation *vs.* γ-irradiation[5–12]), diluent,[5,13–16] nitric acid concentration,[17–22] and temperature[14] have been studied. It appears that irradiation of TBP in alkane diluents in contact with aqueous nitric acid solution produces dibutyl phosphoric acid (HDBP), monobutylphosphoric acid (H_2MBP), phosphoric acid (H_3PO_4), higher molecular weight dimers, acidic phosphates, hydroxylated and nitro-substituted phosphates, and low-molecular weight acid phosphates.[23–28] Among these products, HDBP, H_2MBP, H_3PO_4 and low-molecular weight acid phosphate species are generated by decomposition of the TBP radical cation produced by irradiation stresses or by hydrogen atom abstraction of TBP or the primary radiolysis products. Likewise, diluent decomposition leads to the formation of nitro-substituted alkanes in presence of nitrates and alkane oxidation products such as ketones and carboxylic acids while high-molecular weight products are formed by radical-addition reactions. Without treatment, accumulation of degradation products in the solvent could lead to (i) change of the physicochemical properties of the solutions (density and viscosity),[29] (ii) crud formation,[30–35] and (iii) changes in the extraction properties of the solvent (efficiency, selectivity, *etc.*).[15,19,30,31,36–40]

In the literature, a particular interest has been focused on the complexing properties of the degradation products towards U(VI),[9,39,41,42] Pu(IV),[6,9,42–46] Zr(IV),[30,32,35,45,47–55] Ln(III),[56,57] Fe(III)[58,59] as well as Ru.[37] Few studies have reported the effect of irradiation on the palladium behaviour.[12,19,36,40,58–60] Guedon *et al.*[58,59] reported the formation of a precipitate containing palladium[58] under accelerated degradation conditions (higher than 0.2 MGy) of 30%$_{vol}$ TBP diluted in *n*-dodecane in contact with 3 mol L^{-1} nitric acid. They mentioned that formation of palladium precipitate could be related to diluent degradation. Moreover, Nowak *et al.*[19] showed that solvent degradation is more intense in the presence of palladium(II) during irradiation of 30%$_{vol}$ TBP diluted in *n*-dodecane in contact with nitric acid. In this case, palladium might be involved in the degradation mechanisms of the extraction solvent. Furthermore,

[a]*CEA Marcoule, Nuclear Energy Division, Research Department on Mining and Fuel Recycling Processes (DMRC), BP17171, 30207 Bagnols-sur-Cèze Cedex, France. E-mail: christine.bouyer@cea.fr*

[b]*ORANO Cycle, 1 Place Jean Millier, 92084 Paris La Défense, France*

[c]*DEN, Service de Corrosion et d'étude du Comportement des Matériaux dans leur Environnement (SCCME), CEA, Université Paris-Saclay, 91191, Gif-sur-Yvette, France*

[d]*Université de Lorraine, CNRS, GeoRessources, F-54000 Nancy, France*

† Electronic supplementary information (ESI) available. See DOI: 10.1039/c8ra02695e

degradation is accompanied by an increase of the distribution ratio of Pd(II) (D_{Pd}).[40] In order to explain this behaviour, the effect of some degradation products on the distribution ratio of Pd(II) were investigated.[40,60] The presence of alkenes and butyric aldehyde could be responsible for the increase of D_{Pd}. Conversely, no significant increase in the distribution ratio of palladium(II) was observed when HDBP, H_2MBP, methyl-ethyl ketone, 2-butanol, or iodoethane were added to the extraction solvent. Beside the increase of the distribution ratio of palladium(II), the formation of a black precipitate was also observed. According to the authors, such a precipitate could result from the reduction of Pd(II) into Pd(0) during the oxidation of alkenes into carbonyl compounds.[61]

In the ORANO La Hague reprocessing plants, after two or three decades of industrial operations, it is essential to learn how to cope with aging equipment in order to avoid process dysfunctions. In particular, precipitates containing a high proportion of palladium (>50%$_w$) and carbon (>25%$_w$) were found to be responsible for partial equipment clogging.[62] Because of the high radioactivity of these solids, a thorough characterization is difficult to conduct. Therefore, in order to investigate the phenomena responsible for precipitate formation in the presence of Pd(II) in nuclear fuel reprocessing plants, inactive precipitates were synthetized in the laboratory by contacting 30%$_{vol}$ TBP diluted in TPH with palladium(II) nitrate in 3 mol L^{-1} nitric acid solution under γ-irradiation with a ^{60}Co source. X-Ray Diffraction (XRD) diagrams and InfraRed (IR) spectra of these inactive precipitates have demonstrated similarities between these precipitates and the solids observed in the ORANO plant.[62] These solids have been thoroughly characterized in this work by X-Ray Diffraction (XRD), Thermal Gravimetric Analysis coupled with a Differential Scanning Calorimeter (TGA-DSC), X-ray Photoelectron Spectroscopy (XPS), InfraRed (IR), RAMAN and Nuclear Magnetic Resonance (NMR) spectroscopy as well as ElectroSpray Ionization Mass Spectrometry (ESI-MS). Finally, mechanisms responsible for precipitate formation have been discussed.

Results

A biphasic system composed of 30%$_{vol}$ TBP diluted in TPH in contact with nitric acid solution containing palladium(II) nitrate was irradiated under accelerated degradation conditions of the PUREX process. Such conditions lead to the formation of two solids as illustrated in Fig. 1.

A thorough characterization of the two precipitates $\Phi_{S,1}$ and $\Phi_{S,2}$ was undertaken using complementary analytical techniques such as XRD, TGA, XPS and IR spectroscopy. Additional information has been deduced by dissolving the precipitates in appropriate solvents and by analysing them by NMR, IR and RAMAN spectroscopy as well as ESI-MS spectrometry.

Direct analysis of the precipitates

Samples were analysed by X-Ray Diffraction (XRD) to gain information about their structure. Fig. 2 shows XRD patterns of precipitate $\Phi_{S,1}$, located at the liquid–liquid interface (green line) and the precipitate $\Phi_{S,2}$ located at the bottom of the aqueous phase (blue line).

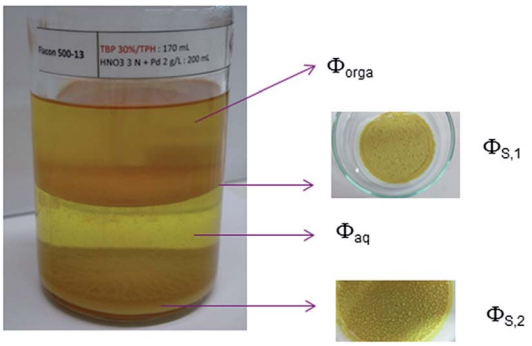

Fig. 1 Formation of two precipitates ($\Phi_{S,1}$ and $\Phi_{S,2}$) after γ-irradiation at 500 kGy with ^{60}Co source of the biphasic system. Initial composition of the organic phase: 30%$_{vol}$ TBP diluted in TPH; initial composition of the aqueous phase: 0.02 mol L^{-1} palladium(II) nitrate in 3 mol L^{-1} nitric acid; organic : aqueous phase ratio = 1 : 1.

Both precipitates have the same crystallographic structure as they exhibit four peaks located at $2\theta = 18.1°$, 26.5°, 36.2°, 40.8° as well as 18.1°, 26.2°, 36.1° and 41.2°, respectively. A comparison of XRD patterns with the literature data indicates that the crystallographic structure of these precipitates is close to that of $Pd(CN)_2 \cdot 0.29H_2O$.[63] Usually in an X-ray powder diffraction pattern, peak intensity and resolution (full-width half maximum) are related to the crystallinity state of the materials (crystallite size and micro-deformation of the crystal lattice). In Fig. 2, the width full-width half maximum of $\Phi_{S,1}$ and $\Phi_{S,2}$ are different: a finer and a higher intensity is observed for $\Phi_{S,2}$ because the precipitate $\Phi_{S,2}$ is probably better crystallized than the precipitate $\Phi_{S,1}$.

The lattice structure of $\Phi_{S,1}$ and $\Phi_{S,2}$ is $I4_1/amd$ and the lattice parameters are $a = b = 4.949(29)$ Å and $c = 8.486(68)$ Å ($R_{Bragg} = 3.18$, $R_{wp} = 0.383$) as well as $a = b = 4.949(29)$ Å and $c = 8.788(85)$ Å ($R_{Bragg} = 3.35$, $R_{wp} = 0.336$), respectively. The lattice parameters a, b and c are the same for both precipitates, but they are smaller than for the commercial compound $Pd(CN)_2 \cdot 0.29H_2O$ ($a = b = 5.119$ Å and $c = 13.600$ Å). $Pd(CN)_2 \cdot 0.29H_2O$ and $Pd(CN)_2 \cdot 0.29NH_3$ contain water and NH_3 molecules to terminate the periodic structure of the solid, respectively (see Fig. 3 for the sake of illustration in the case of $Pd(CN)_2 \cdot 0.29H_2O$).[63] The differences observed between the lattice

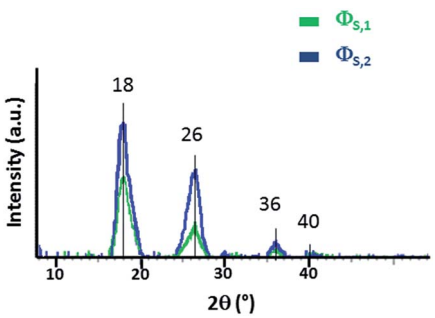

Fig. 2 XRD patterns of (a) $\Phi_{S,1}$ (green color), $\Phi_{S,2}$ (blue color).

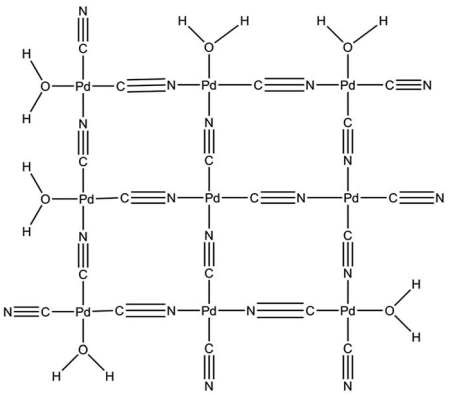

Fig. 3 Chemical structure proposed for $Pd(CN)_2 \cdot xH_2O$ based on $Pt(CN)_2 \cdot 0.67H_2O$ proposed by Hibble.[63]

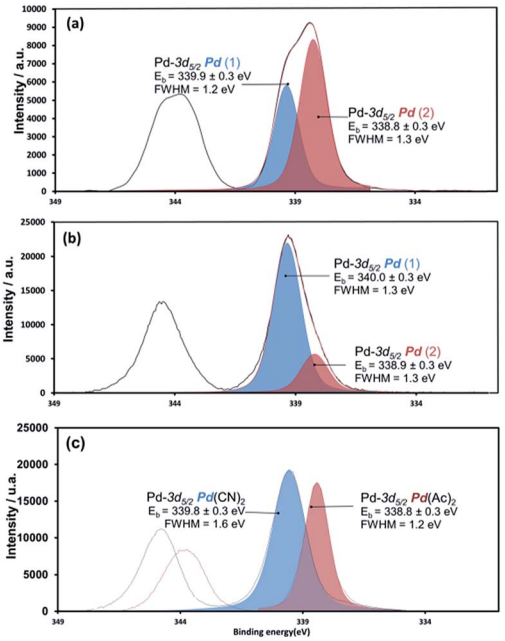

Fig. 4 XPS core level spectra Pd-3d of (a) $\Phi_{S,1}$, (b) $\Phi_{S,2}$ and (c) commercial compounds (in red palladium acetate and in blue palladium cyanide).

parameter c for $\Phi_{S,1}$, $\Phi_{S,2}$ and $Pd(CN)_2 \cdot 0.29H_2O$ may be explained by difference in crystal network. For instance, it can be expected that water molecules located at the outer edges in the $Pd(CN)_2$ network may be replaced by carboxylates groups in $\Phi_{S,1}$ and $\Phi_{S,2}$. Furthermore, the difference in lattice parameters may be explained by the presence of at least two compounds in the precipitate since inclusions of a second compound (in minor quantity) could modify the lattice parameter c.

In order to determine the surface elemental composition of the precipitate, X-ray photoelectron spectroscopy (XPS) was used. This technique provides information about surface composition of solids, their chemical environments and their oxidation states. The Pd-3d, C-1s and N-1s XPS spectra of $\Phi_{S,1}$ and $\Phi_{S,2}$ were recorded and compared with spectra of commercial compounds such as palladium acetate, palladium acetylacetonate, palladium pivalate and palladium cyanide. Atoms of Pd, C, O, N and P are present in both precipitates. Fig. 4 shows the Pd-3d core level spectra of the precipitates. It appears that the elemental composition and the nature of the chemical functions in $\Phi_{S,1}$ and $\Phi_{S,2}$ are similar. Table 1 depicts the binding energies of Pd-$3d_{5/2}$, N-1s and C-1s contributions for both precipitates and the reference samples.

Two different palladium species may be present in the precipitates since XPS spectra exhibit two contributions for Pd-$3d_{5/2}$. The comparison between reference samples and precipitates indicates the presence of Pd(II) bonded to –C≡N and O=C–O– groups. The presence of these two functions is confirmed by the C-1s core level spectra (Fig. S1, in ESI†): two contributions are observed at 286.3 eV for C≡N group and 289.0 eV for O=C–O group, respectively. In addition, NR_4^+ compound is likely present in the precipitates (R = hydrocarbon chain). Indeed, the presence of a peak located at a binding energy of 401.9 eV in the N-1s XPS data is consistent with the presence of ammonium type compound in the precipitates.[64] These results confirm the presence of cyanide groups in close interaction with palladium but also show the presence of other interactions between palladium and carboxylate and/or ammonium groups. The calculation of the Pd/N atomic ratios by considering Pd and N bounded to cyano functions demonstrates that CN groups coordinate only palladium in $\Phi_{S,1}$ and $\Phi_{S,2}$, since Pd/N ratio are the same for the precipitates and commercial $Pd(CN)_2$ (Table 2). Finally, by assuming that Pd is only surrounding by two different environments (Pd–CN and Pd–O–C=O), the proportion of Pd in Pd-cyano and Pd–O=C–O can be calculated for $\Phi_{S,1}$ and $\Phi_{S,2}$ (Table 3). The composition of the two precipitates is slightly different, *i.e.* $\Phi_{S,1}$ contains less Pd linked to CN^- than $\Phi_{S,2}$.

IR spectroscopy was then used to identify the functional groups involved in the precipitates. The IR spectra of (a) $\Phi_{S,1}$ and (b) $\Phi_{S,2}$ precipitates were analyzed and compared with the IR spectra of (c) palladium acetylacetonate, (d) palladium cyanide, (e) palladium acetate and (f) palladium pivalate (Fig. 5). The different bands are assigned in Table 4.

$\Phi_{S,1}$ and $\Phi_{S,2}$ exhibit the same vibration bands. The latter are very similar to those observed in the $Pd(CN)_2$ commercial compound. In particular, the vibration bands at 2220 cm^{-1} (C≡N), 551 cm^{-1} (Pd–N or Pd–C), 464 cm^{-1} (Pd–N or Pd–C) and 264 cm^{-1} (Pd–N) observed for the three compounds seem to confirm that $\Phi_{S,1}$ and $\Phi_{S,2}$ contain $Pd(CN)_2$. The vibration band around 1610 cm^{-1} may indicate the presence of O–C=O functions in $\Phi_{S,1}$ and $\Phi_{S,2}$ as this band is also observed in the spectrum of commercial palladium acetate, palladium pivalate and palladium acetylacetonate, which contain O–C=O group (Fig. 5). The presence of the O–C=O group is in agreement with the previous XPS results, which showed the presence of carboxylate groups in both precipitates. A comparison of the spectra of the precipitate, palladium acetate, palladium pivalate and palladium acetylacetonate shows a slight shift of the band located at 1610 cm^{-1}. However, IR can only confirm the presence of carboxylate group in the compound without giving its exact composition.

Table 1 Binding energies (in eV) of Pd 3d, C-1s and N-1s for $\Phi_{S,1}$, $\Phi_{S,2}$, palladium acetate, palladium pivalate, palladium acétylacétonate and palladium cyanide. The environment of each element is given in brackets[a]

Compound	Binding energy (eV) Pd $3d_{5/2}$	N-1s	C-1s
$\Phi_{S,1}$	338.8 ± 0.3 (**Pd**(OCO) 339.9 ± 0.3 (**Pd**(CN))	399.8 ± 0.3 (Pd(**C**N)$_2$) 401.9 ± 0.3 (*)	286.4 ± 0.3 (**C**≡N) 289.0 ± 0.3 (C–**C**OO)
$\Phi_{S,2}$	338.9 ± 0.3 (**Pd**OCO) 340.0 ± 0.3 (**Pd**(CN))	399.8 ± 0.3 (Pd(**C**N)$_2$) 401.9 ± 0.3 (*)	286.3 ± 0.3 (**C**≡N) 289.0 ± 0.3 (C–**C**OO)
Palladium acetate 	338.8 ± 0.3 (**Pd**($OCOCH_3$))	—	285.6 ± 0.3 (**C**–COO) 286.5 ± 0.3 (**C**–O)
Palladium pivalate 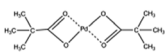	338.7 ± 0.3 (**Pd**($OCOC(CH_3)_3$)	—	289.0 ± 0.3 (C–**C**OO) 285.8 ± 0.3 (**C**–COO)
Palladium acetylacetonate 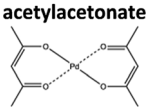	339.0 ± 0.3 (**Pd**(OC_5H_7O))	—	288.7 ± 0.3 (C–**C**OO) 285.8 ± 0.3 (**C**–CO)
Palladium cyanide N≡C—Pd—C≡N	339.8 ± 0.3 (**Pd**(CN)$_2$)	399.6 ± 0.3 (Pd(**C**N)$_2$)	286.1 ± 0.3 (**C**≡N)

[a] *Pd–NR_4^+: attributionbased on the ref. 64.

Table 2 Pd/N atomic ratio determined by XPS

Ratio	Commercial compound Pd(CN)$_2$	$\Phi_{S,1}$	$\Phi_{S,2}$
Pd/N	0.64	0.38	0.67

$\Phi_{S,1}$, $\Phi_{S,2}$ and the commercial compound Pd(CN)$_2$ were analysed by thermogravimetric analysis coupled with a differential scanning calorimeter (TGA-DSC) (Fig. 6). The thermal behaviour of $\Phi_{S,1}$ and $\Phi_{S,2}$ are quite close. Two endothermic peaks observed between 25 °C and 110 °C, and between 350 °C and 650 °C as well as an exothermic peak located between 110 °C and 350 °C accompanied by weight loss were observed. The reaction between 25 °C and 110 °C, and between 110 °C and 350 °C can be attributed to water vaporization[63] and release of organic functions,[67,68] respectively. The weight loss between 350 °C and 650 °C may correspond to the release of $(CN)_{2(g)}$.[63] TGA analyses are consistent with the previous results: the precipitates may be composed of palladium cyanide and organic compounds.

Table 3 Palladium/CN and Pd/O–C=O ratios in $\Phi_{S,1}$ and $\Phi_{S,2}$ deduced by XPS

Sample	Pd–CN	Pd–O=C–O
$\Phi_{S,1}$	41	59
$\Phi_{S,2}$	80	20

TGA analyses allow calculating moisture content in the precipitates (% Moisture). Likewise, it is also possible to calculate the weight percentage of palladium in the precipitates ($\%_w$ Pd) by considering a complete degradation of the product when samples are heated at 650 °C in nitrogen atmosphere. At this temperature, there is no additional organic matter in the precipitate and the weight of the sample corresponds to the weight of palladium. Moreover, the weight of organic ($\%_w$ organic) and cyanogen ($\%_w$ $(CN)_2$) can also be calculated. Finally, the weight percentage of Pd-cyano groups ($\%_w$ $Pd_{(CN)2}$) and Pd-carboxylate groups ($\%_w$ $Pd_{(O-C=O)}$) in $\Phi_{S,1}$, $\Phi_{S,2}$ and

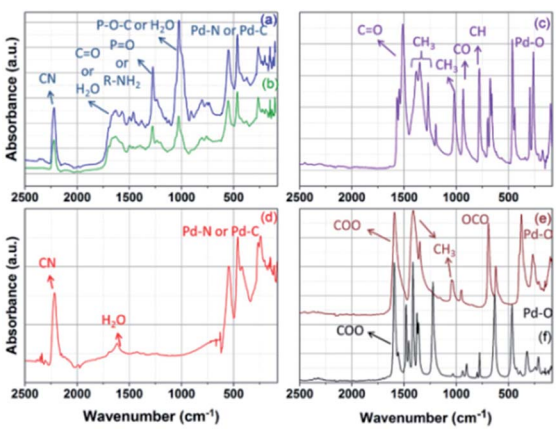

Fig. 5 IR spectra of (a) $\Phi_{S,1}$ (b) $\Phi_{S,2}$, (c) palladium acetylacetonate, (d) palladium cyanide, (e) palladium acetate and (f) palladium pivalate.

Table 4 Identification of the main vibration bands observed in the IR spectra of $\Phi_{S,1}$, $\Phi_{S,2}$, $\Phi_{S,3}$, palladium cyanide, palladium acetate, palladium acetylacetonate and palladium pivalate and their attribution. w = weak; m = medium; s = strong

	Wavenumber (cm^{-1})						
Assignment	$\Phi_{S,1}$	$\Phi_{S,2}$	$\Phi_{S,3}$	Palladium cyanide[63]	Palladium acetate[65]	Palladium acetylacetonate[66]	Palladium pivalate
H_2O or amine + CH_3, as stretch	3680 to 2999 (m)	3679 to 2991 (m)	3378 to 3015 (w)	—	2937 (w)	2921 (w)	
$CH–CH_{alkane}$	2960 to 2870 (w)	2956 to 2870 (w)	2975 to 2827 (w)	—			
C≡N	2221 (m)	2221 (m)	—	2218 (m)			
H_2O or O–C=O	1610 (m)	1610 (m)	1610 (s)	1616 (w)	1593 (s)	1565 (m)	1595 (s)
P–O–C or H_2O	1028 (s)	1028 (s)	1022 (s)	—			
Pd–N or Pd–C	551 (m)	551 (m)	—	547 (s)			
Pd–N or Pd–C, Pd–O	464 (m)	464 (m)	—	462 (s)		462 (s)	466 (s)
Pd–N, Pd–O, OPdO	266 (w)	264 (w)	—	266 (s)	268 (m)	262 (m)	

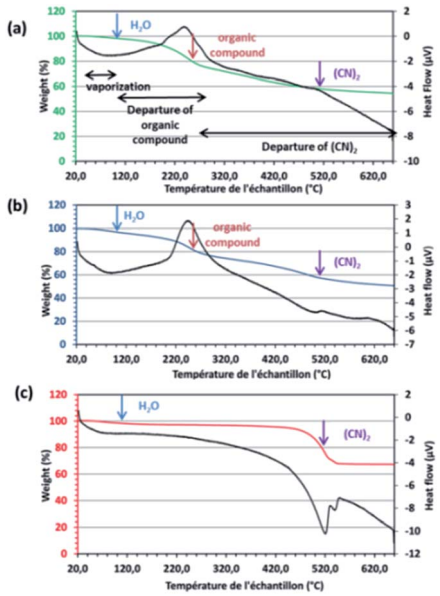

Fig. 6 TGA thermograms of (a) $\Phi_{S,1}$ (in green), (b) $\Phi_{S,2}$ (in blue) and (c) $Pd(CN)_2$,0.29H_2O (in red). Black line: heat flow (µV); measurements performed in nitrogen atmosphere.

$Pd(CN)_2$ can be deduced from TGA experiments by using the calculation method reported in the experimental part (eqn (13) and (14)). Table 5 reports these values.

The moisture contents are similar in the precipitates (2–3% for water). Moreover, total palladium contents are in the same order of magnitude in the solids $\Phi_{S,1}$ and $\Phi_{S,2}$ (around 54–57% for Pd). The major difference in composition between $\Phi_{S,1}$ and $\Phi_{S,2}$ is the distribution between the CN^- group and COO^- group. $\Phi_{S,2}$ contains more palladium coordinated to CN^- than $\Phi_{S,1}$ (55% *vs.* 39%). Conversely, more palladium coordinated to carboxylate group is observed in $\Phi_{S,1}$ than $\Phi_{S,2}$. Although the distribution of Pd species determined by TGA-DSC is slightly different from that calculated from XPS data (see Table 3), both techniques show that more Pd is linked to CN^- in $\Phi_{S,2}$ than in $\Phi_{S,1}$. This difference could be due to the difficulty by TGA-DSC to quantify precisely the $(CN)_{2(g)}$ release between 350 °C and 650 °C in $\Phi_{S,1}$ and $\Phi_{S,2}$. In the commercial compound $Pd(CN_2)$, the loss in mass of $(CN)_{2(g)}$ is well defined in TGA-DSC data, whereas a broad signal is observed for the precipitates. Moreover, the XPS analysis allows analysing the extreme surface of the powder only. Some errors can come from the choice of the background, the recombination of the spectra and a different depth of analysis from one sample to another.

Analysis of the precipitates after solubilisation

Direct analyses of the precipitates by IR, Raman and XPS showed that Pd is coordinated to CN^- and COO^- while NR_4^+ groups may be present in the precipitates. However, it is impossible to confirm the exact number of palladium and organic complexes

Table 5 Quantitative analyses of the precipitates and $Pd(CN)_2 \cdot xH_2O$ by TGA-DSC, *i.e.* weight percentages of moisture (% Moisture), palladium ($\%_w$ Pd), cyanogen ($\%_w$ $(CN)_2$), organic compounds ($\%_w$ organic)in $\Phi_{S,1}$, $\Phi_{S,2}$ and the commercial palladium cyanide. Calculation of the distribution Pd species in the precipitates: $\%_w$ $Pd_{(CN)2}$ corresponds to palladium coordinated to CN group and $\%_w$ $Pd_{(O-C=O)}$ corresponds to palladium coordinated to carboxylate group

Sample	$\%_w$ Moisture (between 25 °C and 110 °C)	$\%_w$ Pd (at 650 °C)	$\%_W$ $(CN)_2$ (between 350 and 650 °C)	$\%_W$ Organic (between 110 and 350 °C)	$\%_w$ $Pd_{(CN)2}$	$\%_w$ $Pd_{(O-C=O)}$
$\Phi_{S,1}$	3	54	10	33	39	61
$\Phi_{S,2}$	3	57	16	24	55	45
$Pd(CN)_2 \cdot xH_2O$	2	68	30	—	94	—

present in the precipitates. In order to deeply characterize the precipitates, they were dissolved in several solvents (DMSO (dimethyl sulfoxide), NH_3 (1 mol L^{-1}), pyridine) and the obtained solutions were analysed. It was expected that NH_3 would be able to dissolve the precipitates as $Pd(CN)_2$ can be dissolved in NH_3 by forming the soluble complex $Pd(CN)_2(NH_3)_2$.[69] After 15 minutes of stirring of 20 mg of precipitate in 10 mL of 1 mol L^{-1} NH_3, a filtrate (Φ_{F1}) and an insoluble fraction ($\Phi_{S,3}$) were obtained. The insoluble fraction $\Phi_{S,3}$ and the filtrate Φ_{F1} were then analysed by IR and Raman spectroscopy (Fig. 7).

The corresponding vibration bands are reported in Table 4. These spectra show the presence of vibration bands at 2218 cm^{-1} (C≡N), 551 cm^{-1}, 464 cm^{-1}, and 266 cm^{-1} (Pd–N or Pd–C) in $\Phi_{S,1}$. These bands have not been observed in $\Phi_{S,3}$. Therefore, this study confirms that 1 mol.L^{-1} NH_3 allows solubilizing $Pd(CN)_2$. Moreover, further XPS analyses performed on the $\Phi_{S,3}$ fraction confirm that NH_3 totally dissolved $Pd(CN)_2$ since the Pd contribution located at 339.3 eV has disappeared (Fig. S2, ESI†). This conclusion was also confirmed by Raman spectroscopy on the filtrate Φ_{F1}, since two vibration bands located at 2149 and 2140 cm^{-1} attributed to cyano groups were observed (Fig. 8).

Furthermore, the presence of an insoluble fraction $\Phi_{S,3}$ (partial dissolution of $\Phi_{S,1}$ in NH_3 1 mol L^{-1}) seems to show that the precipitate is composed of at least of two different compounds. The second compound contains H_2O molecules (vibration bands 3680–3379 cm^{-1} and 1610 cm^{-1}), CH–CH groups (vibration bands at 2975 and 2827 cm^{-1} assigned to CH–CH_{alkane} vibration), O–C=O functions (vibration band at 1610 cm^{-1}), phosphate groups (vibration bands at 1274 cm^{-1}, 1022 cm^{-1}) or R–NH_2 functions (vibration bands at 1274 cm^{-1}).

ESI-MS experiments were undertaken to characterize the precipitates after dissolution in pyridine. This technique allows the transfer of pre-existing ions from the solution into the gas phase in order to obtain speciation information. Fig. 9 shows ESI-MS spectra obtained after partial dissolution in pyridine of $\Phi_{S,1}$, $\Phi_{S,2}$ and the commercial compound $Pd(CN)_2$. The main ions containing Pd were identified by comparison with a calculated isotopic pattern (Table 6).

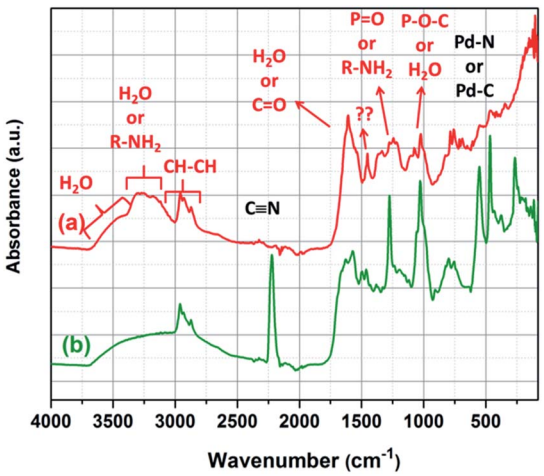

Fig. 7 IR spectra of (a) $\Phi_{S,3}$ (solid residue after dissolution of the $\Phi_{S,1}$ in 1 mol L^{-1} NH_3) and (b) $\Phi_{S,1}$.

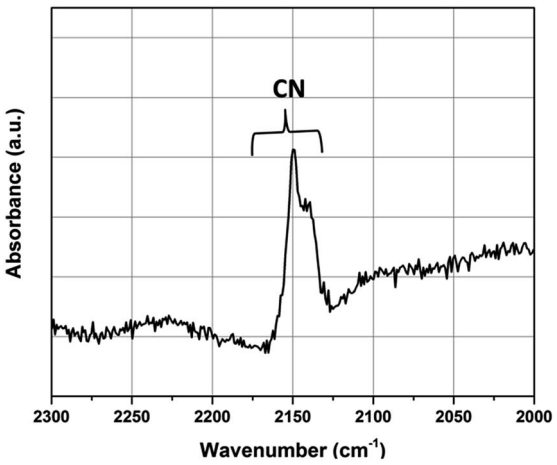

Fig. 8 Raman spectrum of Φ_{F1} obtained after dissolution of $\Phi_{S,1}$ in NH_3 (1 mol L^{-1}) at a solid : liquid ratio of 9 (mass of precipitate in g/volume of solvent in L).

Most ions contain pyridine indicating a strong solvation of Pd by pyridine during the solubilisation step. Moreover, the presence of ions of m/z = 180.4–188.9, 259.9–268.9, 285.9–294.8, 294.8–303.9, 313.1–322.0, 496.0–509.0 and 552.2–561.2 assigned to $Pd(pyr)^+$ (pyr = C_5H_5N), $Pd(pyr)_2^+$, $Pd(pyr)_2(CN)^+$, $Pd(pyr)_2OH(H_2O)^+$ $Pd(pyr)_2OH(H_2O)_2^+$, $Pd_2(pyr)_3(CN)_2^+$, and $Pd^I(pyr)_2(CN)(TBP)^+$ indicates the partial reduction of Pd(II) into Pd(I). Nevertheless, it is not possible to say if Pd reduction occured during the dissolution step of the solid in pyridine or during the de-solvation/ionization step. The ions of m/z = 259.9–268.9, 285.9–294.8, 294.8–303.9, 523.0–533.9 and 601.1–614.0 corresponding to $Pd(pyr)_2^+$, $Pd(pyr)_2(CN)^+$, $Pd(pyr)_2OH(H_2O)^+$, $Pd_2(pyr)_3(CN)_3^+$ and $Pd_2(pyr)_4(CN)_3^+$, respectively, were present in both the commercial compound and the precipitates $\Phi_{S,1}$ and $\Phi_{S,2}$. The ions of m/z = 313.1–322.0 and 610.9–622.9 assigned to $Pd(pyr)_2OH(H_2O)_2^+$ and

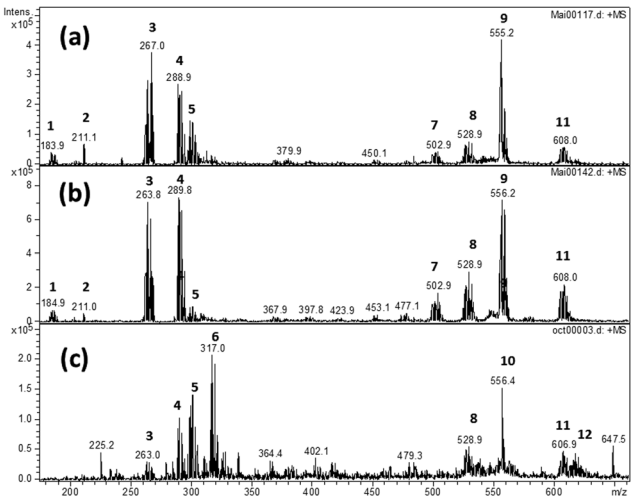

Fig. 9 ESI-MS spectra of (a) $\Phi_{S,1}$, (b) $\Phi_{S,2}$ and (c) $Pd(CN)_2$ after partial dissolution in pyridine (solid : liquid ratio = 2 g L^{-1}) and dilution in acetonitrile ((a) 1/10th, (b) 1/100th and (c) 1/10th). Experiment conditions: trap drive setting = 50; skimmer voltage = 30 V.

$Pd_2(pyr)_4(CN)_2OH(H_2O)^+$, respectively, were only observed after dissolution of the $Pd(CN)_2$ commercial compound whereas the ions of *m*/*z* equal to 259.9–268.9, 267.8, 523.0–533.9, 552.2–561.2, 555.2 and 601.1–614.0 assigned to $Pd(pyr)_2^+$, $(TBP)H^+$, $Pd_2(pyr)_3(CN)_2^+$ $Pd^I(pyr)_2(CN)(TBP)^+$, $(TBP)_2Na^+$, and $Pd_2(pyr)_4(CN)_3^+$, respectively, were observed after dissolution of the precipitates in the pyridine. Thus, some differences are observed between the solution obtained after solubilisation of the commercial $Pd(CN)_2$ compound and the precipitates. Moreover, the ion of *m*/*z* equal to 556.4 observed in the commercial compound does not contain palladium and may be due to the presence of an organic impurity because of the very high sensitivity of the technique.

In the $Pd(CN)_2$ commercial compound, each palladium atom is surrounded by four CN groups. However, some water molecules can terminate the periodic structure (see Fig. 3). During the solubilisation step, pyridine molecules solvate the palladium and replace some CN group to produce $Pd_2(pyr)_4(CN)_3^+$ and $Pd_2(pyr)_4(CN)_2OH(H_2O)^+$. Then, during the transfer from the solution to the gas phase in the mass spectrometer, these ions can be modified by release of a pyridine, CN group or water molecules and Pd(II) could be reduced so that $Pd_2^{II}(pyr)_4(CN)_3^+$; $Pd_2^{II}(pyr)_3(CN)_3^+$. $Pd^I(pyr)_2OH(H_2O)_2^+$; $Pd^I(pyr)_2OH(H_2O)^+$; $Pd^I(pyr)_2CN^+$ and $Pd^I(pyr)_2^+$ can be formed.

After solubilisation of the precipitates, the ions $Pd_2(pyr)_4(CN)_2OH(H_2O)^+$ and $Pd^I(pyr)_2OH(H_2O)_2^+$ were not observed. However, the ions $Pd^I(pyr)_2(CN)(TBP)^+$, $(TBP)_2Na^+$ and $(TBP)H^+$ were observed and indicate the presence of the TBP in the solution. The presence of HDBP was also confirmed since an ion of $m/z = 211.1$ which corresponds to $(HDBP)\text{-}H^+$ is observed. Comparing to the commercial compound in which water molecules terminate the periodic structure, it is possible that in the precipitate some TBP molecules terminate the structure. Thus, although not conclusive in providing structural information for the solid, the ESI-MS results provide evidence that the presence of TBP in the precipitates.

In order to get information about the chemical structure of the precipitates 1D and 2D ^1H NMR spectra were recorded after $\Phi_{S,2}$ dissolution in DMSO-D6 (deuterated DMSO). Pyridine was not used for NMR analyses in spite of the high solubilization power of pyridine because of the two following drawbacks: (i) pyridine peak overlap ^1H signal in the aromatic area (about 7 ppm) and (ii) pyridine can easily dissociate Pd species. The 1D ^1H NMR spectrum of $\Phi_{S,2}$ exhibits the reference peak at 0 ppm (TMS) and a peak located at 2.5 ppm attributed to residual protons of DMSO-D6 (Fig. 10). The triplet and the three multiplets located at 0.85, 1.31, 1.53 and 3.82 ppm, respectively, correspond to the butyl protons in TBP (for more information ESI – Fig. S3 and S4†). The three symmetric peaks of same intensity centred at 7.05 ppm indicate protons coupling with a nucleus of spin 1 (Fig. 10). Among the nuclei in the sample, only the nitrogen has a spin 1. The corresponding $J_{^{14}N^1H}$ coupling constant of 104 Hz is in the magnitude order of $^1J_{NH}$ (*i.e.* ^1H one bond apart from ^{14}N) and consequently could be due to the presence of an amine function.

In order to confirm the presence of amine functions in the precipitate $\Phi_{S,2}$, a biphasic system composed of 30%$_{vol}$ TBP diluted in TPH contacted with 3 mol L^{-1} nitric acid solution containing palladium nitrate (5 g L^{-1} Pd) and $NaNO_3$ (66 g L^{-1}) enriched with 98% atomic ^{15}N was irradiated and the aqueous phase was analyzed. The ^{15}N NMR spectrum shows a triplet centred on −360 ppm (^{15}N scale is referenced to $CH_3\text{–}NO_2$) that is characteristic of NH_2 functions (Fig. S5, ESI†). The 2D $^{15}N\text{–}^1H$ spectrum displayed in Fig. S7 (ESI†) shows a correlation spot ($^1J_{^{15}N^1H} = 72$ Hz) between the triplet at −360 ppm observed in the ^{15}N NMR spectrum (Fig. S7†) and the peak located at 6.1 ppm observed in the ^1H NMR spectrum (Fig. S6 in ESI†). Therefore, protons observed at 6.1 ppm corresponds to NH_2 functions. Likewise, the peaks centred at 7.05 ppm in the ^1H NMR spectrum of $\Phi_{S,2}$ can be assigned to an amine function.

To complete ^1H NMR peak assignments for $\Phi_{S,2}$, gHSQCAD and gHMBCAD pulse sequences were performed. These 2D

Table 6 *m*/*z* ratios and Pd species assignments in ESI-MS (positive ionization mode) for $\Phi_{S,1}$, $\Phi_{S,2}$ and $Pd(CN)_2$ in pyridine. pyr = pyridine = C_5H_5N; TBP = tri-*n*-butylphosphate = $C_{12}H_{27}O_4P$. Peak numbers ($N°$) are reported in Fig. 9[a]

$N°$ (Fig. 9)	*m*/*z* pattern	Identification	$Pd(CN)_2$	$\Phi_{S,1}$	$\Phi_{S,2}$
1	180.4–188.9	$Pd^I(pyr)^+$	—	*	*
2	211.1	$(HDBP)H^+$	—	*	*
3	259.9–268.9	$Pd^I(pyr)_2^+$	*	*	*
	267.8	$(TBP)H^+$	—	*	*
4	285.9–294.8	$Pd^I(pyr)_2(CN)^+$	*	*	*
5	294.8–303.9	$Pd^I(pyr)_2OH(H_2O)^+$	*	*	*
6	313.1–322.0	$Pd^I(pyr)_2OH(H_2O)_2^+$	*	—	—
7	496.0–509.0	$Pd^IPd^{II}(pyr)_3(CN)_2^+$	—	*	*
8	523.0–533.9	$Pd_2^{II}(pyr)_3(CN)_3^+$	*	*	*
9	552.2–561.2	$Pd^I(pyr)_2(CN)(TBP)^+$	—	*	*
	555.2	$(TBP)_2Na^+$	—	*	*
10	556.4	n.i.	*	—	—
11	601.1–614.0	$Pd_2^{II}(pyr)_4(CN)_3^+$	*	*	*
12	610.9–622.9	$Pd_2^{II}(pyr)_4(CN)_2OH(H_2O)^+$	*	—	—

[a] *, observed species; —, non detected species; n.i.: non identified species.

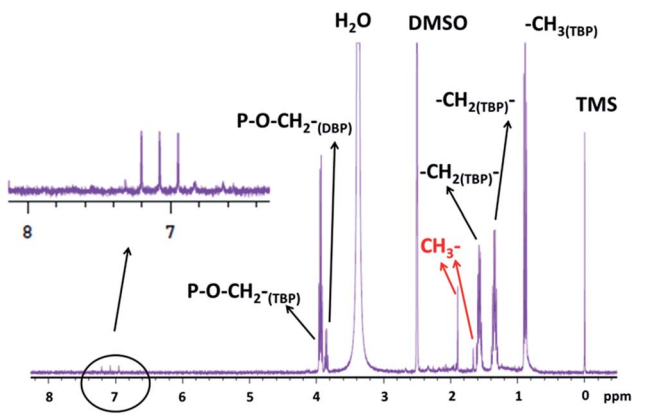

Fig. 10 1D ^1H NMR spectrum of $\Phi_{S,2}$ partially dissolved in DMSO-D6 $m(\Phi_{S,2})$ = 9.8 mg in 650 µL of DMSO-D6, *i.e.* *S*/*L* = 15.07 g of precipitate/L of solvent.

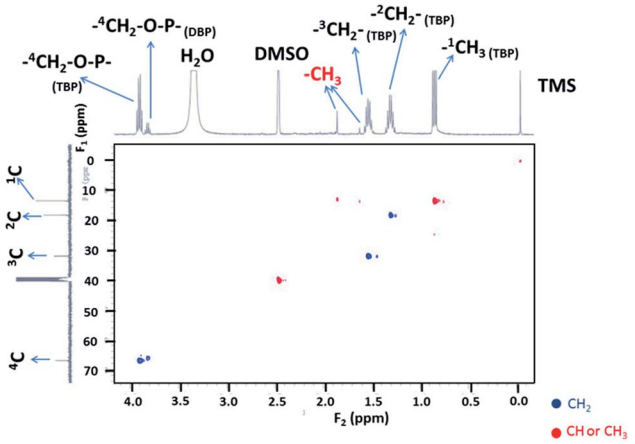

Fig. 11 2D NMR spectrum of ^{1}H and ^{13}C (pulse sequence gHSQCAD) of $\Phi_{S,2}$ partially dissolved in DMSO-D6 with $m(\Phi_{S,2}) = 9.8$ mg in 650 μL of DMSO-D6 ($S/L = 15.07$ g of precipitate/L of solvent).

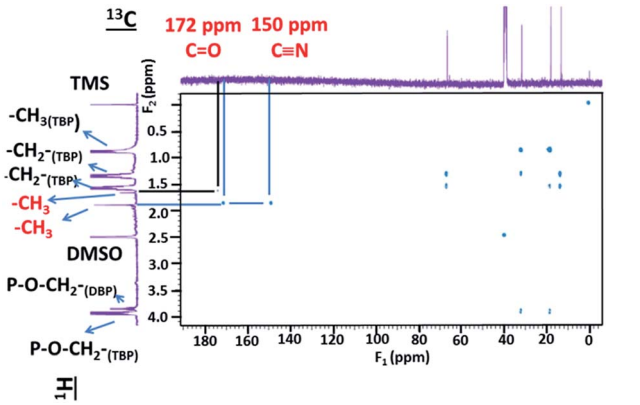

Fig. 12 2D NMR spectrum of ^{1}H and ^{13}C (pulse sequence gHMBCAD) of $\Phi_{S,2}$ partially dissolved in DMSO-D6 with $m(\Phi_{S,2}) = 9.8$ mg in 650 μL of DMSO-D6 ($S/L = 15.07$ g of precipitate/L of solvent).

pulse sequences allow ^{13}C assignments through ^{1}H detections and the corresponding coupling constants: ($^{1}J_{CH}$ for gHSQCAD) and ($^{n}J_{CH}$ with $n = 2$ or 3 for gHMBCAD) (Fig. 11 and 12). In Fig. 11, positive red crosspeaks belong to CH– and $–CH_3$ groups whereas negative blue peaks belong to $–CH_2–$ groups. The two red cross-peaks at (1.6 ppm; 13.8 ppm) (^{1}H scale; ^{13}C scale) and (1.9 ppm; 13.8 ppm) are two unshielded $–CH_3$ groups. At 0.85, 1.31, 1.53 and 3.82 ppm (^{1}H scale), the set of large and small cross peaks are assigned to the $CH_3–$, two $–CH_2–$ and $–CH_2–O–P$ groups at 13.8, 18.6, 32.2 and 67.0 ppm (^{13}C scale) of the butyl chains bearing on TBP (main compound) and HDBP peaks arising from TBP degradation. The presence of TBP or HDBP in the precipitate is consistent with IR and ESI-MS data. On the $^{1}H–^{13}C$ gHMBCAD (Fig. 12), the $–CH_3$ chemical shift located at 1.9 ppm on the 1H scale is correlated to carbon peaks two or three bonds apart at 172 and 150 ppm which are assigned to carbonyl and cyano groups respectively. Such information allows to suggest the presence of methyl-oxo-cyanide in $\Phi_{S,2}$ ($CH_3–CO–CN$). NMR analyses for $\Phi_{S,1}$ have not been undertaken. However, the same results could be expected.

Discussion

In this work, γ-irradiation of a biphasic system containing $30\%_{vol}$ TBP diluted in TPH (organic phase) in contact with palladium(II) nitrate dissolved in 3 mol L^{-1} nitric acid (aqueous phase) led to the formation of a precipitate located at the liquid–liquid interface ($\Phi_{S,1}$) and a precipitate that settled spontaneously ($\Phi_{S,2}$) (Fig. 1). Elemental analyses showed that both precipitates contain palladium. Solubilisation tests demonstrated that the precipitates do not contain only one compound but a mixture of at least two compounds. XRD, XPS, TGA-DSC, IR, ESI-MS and NMR analyses allowed for the identification of palladium cyanide in the precipitates. Other compounds such as palladium carboxylates, phosphates (*i.e.* TBP or HDBP), compounds with ammonium and/or amine functions may also be present to a lesser extent. In the following, the presence of the different compounds in the precipitate is discussed.

The irradiation of a biphasic system leads to both radiolysis of nitric acid and water molecules in the aqueous phase, and radiolysis of the molecules present in the organic phase (TBP and TPH). Radiolysis of nitric acid primarily leads to the formation of HNO_2 (ref. 23 and 70) and H_2O_2 (ref. 70) whereas radiolysis of TBP and TPH can generate many different degradation products such as alkenes, carbonyl compounds (R–CO–R′, R–CO–H), carboxylic acids (R–COOH), alcohols (R–OH), nitro compounds ($R–NO_2$)[23] and phosphorus compounds such as HBDP, H_2MBP, H_3PO_4, *etc.*[26] In addition, several authors mentioned the formation of secondary products, such as oximes (R–C═N–OH), even though this molecule has never been formally identified.[23,71] These oxime compounds have a great affinity for Pd.[72]

NMR and ESI-MS analyses showed the presence of TBP and HDBP in $\Phi_{S,1}$ and $\Phi_{S,2}$ but these molecules may not be directly bonded to the Pd since XPS analyses showed only two different environments around Pd that are not characteristic of phosphorous compounds but rather C≡N and O–C═O groups. However, the presence of TBP and HDBP in the precipitate may also explained by the inclusion of TBP/HDBP molecule in the solid since the precipitate are obtained in the biphasic system containing both TBP and HDBP (due to the radiolytic degradation of the TBP).

Besides, NMR analyses showed the presence of carboxylate and CN group. XPS indicated that these two groups are directly bonded to palladium. The formation of Pd-carboxylate compounds could be easily explained by the reaction of carboxylic acid (radiolytic degradation products of the TBP–alkane solution[73–76]) with the palladium leading to a precipitate.

Regarding the palladium cyanide formation, an assumption would be the reaction of HCN with the palladium present in the organic/aqueous solutions. Ketones and oximes seem to be a valuable precursor to the formation of HCN among the degradation products formed during γ-irradiation.[77,78] In particular, it is interesting to highlight that heating of aldehydes, ketones or alcohols in the presence of hydroxylamine

(NH_2OH) or nitrous acid (HNO_2) in acidic media can be responsible for HCN formation.[77] An oxo-oxime can be formed by the addition of HNO_2 or NH_2–OH to the carbon in α position of the carbonyl group (eqn (1)). This species becomes dehydrated and leads to the formation of an α-keto-cyanide (eqn (2)), which can be hydrolyzed into carboxylic acid (R–CO–OH) with the departure of HCN (eqn (3)).[77]

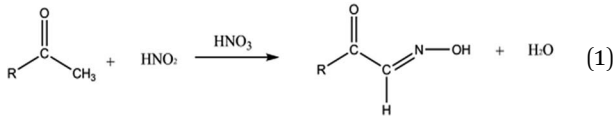
(1)

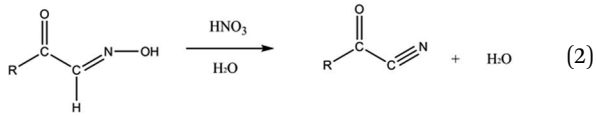
(2)

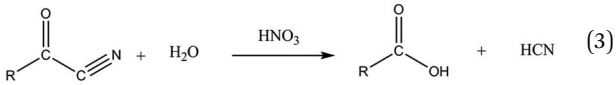
(3)

Other ways to produce oxime that are consistent with the experimental conditions of the PUREX process were also reported in the literature.[77] In presence of HNO_2, alcohols can and form nitrous acid ester by esterification (eqn (4)). A rearrangement can occur to produce a compound containing both an hydroxyl (–OH) and a nitroso (–N=O) groups, *i.e.* an oxime (eqn (5)). The oxime can be afterward hydrolysed into a ketone (eqn (6)). Finally, the ketone can form HCN by reacting with HNO_2 or NH_2OH according to eqn (1) to (3).

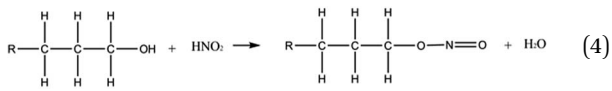
(4)

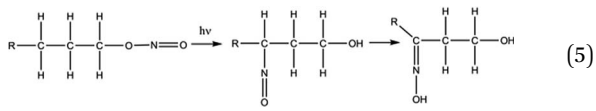
(5)

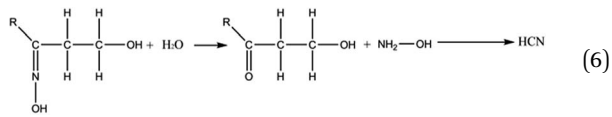
(6)

Another alternative pathway for oxime formation could be the reaction of $CH_3^{\bullet}$ radical with NO (eqn (7)) since NO radicals can be formed by irradiation of TBP or alkanes.[79]

$$CH_3^{\bullet} + NO \rightarrow H_3C{-}N{=}O \rightleftarrows H_2C{=}N{-}OH \quad (7)$$

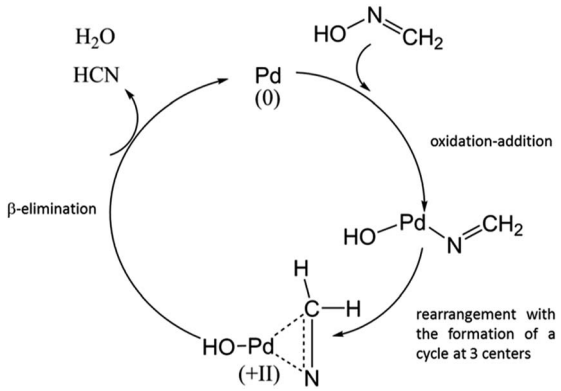

Scheme 1 Proposition of catalytic mechanism for HCN formation in the presence of Pd^0 and formaldehyde oxime.

In this particular case, CH_2=N–OH can lead to the formation of HCN in the presence of Pd(0) according to Scheme 1. The presence of Pd(0) is likely and has already been reported by Vialard and Germain[12] after radiolysis of TBP in alkane solution in contact with aqueous phase.

Finally, HCN can react with Pd^{2+} to form $Pd(CN)_2$ as shown in eqn (8) since the stability constant is quite high ($K = 10^{+41.8}$).[80]

$$Pd^2 + 2HCN = Pd(CN)_2 + 2H^+ \quad (8)$$

Several formation pathways for $Pd(CN)_2$ have been proposed. An organic degradation product, such as alcohol, carbonyl compound or methyl radical, in the presence of HNO_2 or NH_2OH allows the formation of HCN. Then, in presence of Pd^{2+} in solution and HCN, $Pd(CN)_2$ can be formed with a thermodynamic constant of $10^{+41.8}$ (Scheme 2).

Conclusion

XRD, XPS, TGA, IR, ESI-MS and NMR have been used to characterize the two precipitates ($\Phi_{S,1}$ and $\Phi_{S,2}$) produced by γ-irradiation at 500 kGy of 30% $_{vol}$ tri-*n*-butylphosphate diluted in TPH in contact with nitric acid containing palladium(II) nitrate. $\Phi_{S,1}$ and $\Phi_{S,2}$ exhibit similar structures and contain a mixture of $Pd(CN)_2$ and other compounds (Pd-carboxylate, ammonium or amine functions and phosphorous compounds). The degradation products formed during irradiation of the two-phase biphasic system may be responsible for precipitates formation of palladium. Among the degradation products formed by irradiation, ketones and oximes could be responsible for precipitate formation.

Future studies designed to validate the proposed $Pd(CN)_2$ formation mechanism and to identify the other Pd compounds are currently under progress. Nitrate group arising from nitric acid or palladium nitrate may be responsible for the presence of CN^- in the precipitates since only these two products contain nitrogen atoms in the biphasic system. Therefore, γ-irradiation in the presence of $^{15}HNO_3$ may be very helpful to identify the different intermediates involved in HCN formation. Specifically,

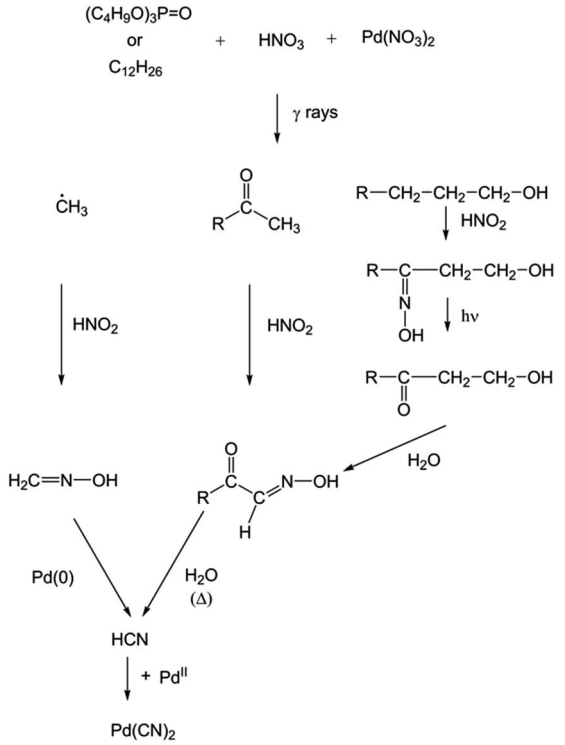

Scheme 2 Proposition of a formation pathway for $Pd(CN)_2$ after irradiation of a biphasic system composed of TBP in alkane in presence of nitric acid solution containing palladium(II) nitrate.

analyses of the organic and the aqueous phases could provide information on the nitrogen species formed by γ-irradiation and allow for the confirmation or invalidation of the proposed mechanism for palladium cyanide formation. Biphasic systems containing an organic phase either of pure TBP or pure dodecane in contact with a nitric acid aqueous solution containing palladium(II) nitrate will be irradiated under the same conditions as the biphasic system {TBP–TPH–HNO_3–Pd} described in this study in order to determine which organic molecule is responsible for the precipitate formation.

Experimental

Reagent

Palladium nitrate (purity = 99.9%, Sigma Aldrich), 68.5%$_{wt}$ nitric acid (purity = 99.8%, VWR), TBP (purity ≥ 99.9%, VWR) and tetrapropylene hydrogen (TPH, petroleum fraction, Novasep) were used without further purification. The extraction solvent was prepared by mixing appropriate amounts of TBP and TPH (30%$_{vol}$ TBP diluted in TPH). Palladium(II) nitrate was weighted in order to obtain a concentration of 0.02 mol L^{-1} (or 2 g L^{-1}) of Pd in 3 mol L^{-1} nitric acid aqueous solution prepared by dilution of 68.5%$_{wt}$ nitric acid in Milli-Q deionized water. The solution was filtered to remove traces of metallic palladium.

Palladium(II) cyanide (purity = 99.9%), palladium(II) acetate (purity ≥ 99.9%) palladium(II) pivalate (purity = 97%), palladium(II) acetylacetonate (purity = 99%) were purchased from Sigma Aldrich and used without further purification.

Dimethyl sulfoxide (DMSO, purity = 99.5%, VWR), pyridine (pyr, purity = 99.7%, VWR), ammonia (purity = 99.8%, VWR), dichloromethane (purity = 99.9%, Sigma Aldrich), tetrahydrofuran (THF, purity ≥ 99.9%, Acros Organic), methanol (purity = 99.8%, VWR), acetone (purity = 99.9%, VWR) were used without further purification.

An aqueous solution of 1 mol L^{-1} sodium hydroxide was purchased from VWR and used for potentiometric titrations.

A palladium solution of 1000 μg mL^{-1} in 10%$_{wt}$ HCl provided by Fischer Scientific was used to prepare the standard solutions for ICP-AES measurement.

Synthesis of the palladium precipitates

A 3 mol L^{-1} nitric acid aqueous phase containing 0.02 mol L^{-1} palladium(II) nitrate (2 g L^{-1} of Pd) was contacted with an organic phase containing 30%$_{vol}$ TBP diluted in TPH with a volume ratio organic to aqueous phase of 1. The organic phase was not pre-equilibrated before extraction of Pd(II). The biphasic system was shaken for 5 minutes at ambient temperature before γ-irradiation to 500 kGy by using a ^{60}Co source at the Synergy Health company (Marseille, France) with a dose rate of about 5 kGy h^{-1}. The integrated dose was chosen to accelerate the degradation process and to simulate long term behaviour of the solvent under irradiation stress. After γ-irradiation of the biphasic system, four phases were observed: an organic phase (Φ_{org}), an aqueous phase (Φ_{aq}), a light precipitate at the liquid–liquid interface ($\Phi_{S,1}$) and a heavy precipitate ($\Phi_{S,2}$) at the bottom of the flask as illustrated in Fig. 1. Precipitates were recovered and filtered under vacuum. Afterwards, they were washed twice with 2 mol L^{-1} nitric acid and dried at 40 °C for 24 hours. The palladium concentration and the acidity of the liquid phases, before and after irradiation are reported Table 7. The acidity of the organic and the aqueous phases scarcely decreased while the palladium concentration in the aqueous phase decreased drastically.

Table 7 Palladium and proton concentrations before and after γ-irradiation at 500 kGy of the biphasic system. Initial composition: 30%$_{vol}$ TBP in TPH in contact with 0.02 mol L^{-1} palladium(II) nitrate in 3 mol L^{-1} nitric acid aqueous phase with an organic:aqueous phase ratio of 1 : 1 (γ-irradiation performed with ^{60}Co)

$[Pd]_{aq}$ (mmol L^{-1})		$[H^+]_{aq}$ (mol L^{-1})		$[H^+]_{orga}$ (mol L^{-1})	
Before irradiation	After irradiation	Before irradiation	After irradiation	Before irradiation	After irradiation
18 ± 10^{-3}	4 ± 10^{-3}	2.63 ± 0.07	2.45 ± 0.07	0.62 ± 0.07	0.60 ± 0.07

Table 8 Volumes of irradiated aqueous phase (V_{aq}) and organic phase (V_{org}), and weights of precipitates $\phi_{S,1}$ and $\phi_{S,1}$ before and after γ-irradiation ($m_{\phi_{S,1}}$ and $m_{\phi_{S,1}'}$ respectively)

Volume of the solutions before irradiation		Weights of precipitates after irradiation	
V_{aq} (mL)	V_{orga} (mL)	$m_{\phi_{S,1}}$ (mg)	$m_{\phi_{S,2}}$ (mg)
200	170	264	312

The volumes of the aqueous and organic phases before γ-irradiation and the weight of the precipitates $\phi_{S,1}$ and $\phi_{S,2}$ recovered after irradiation are reported in Table 8.

In order to characterize the composition of the precipitates, dissolution tests were performed by using DMSO, CH_2Cl_2, THF, methanol, acetone, NH_3 (1 mol L^{-1}) and pyridine. No complete dissolution of $\Phi_{S,1}$ and $\Phi_{S,2}$ with a S/L of 2 (solid/liquid: mass of precipitate (g)/volume of the solvent (L)) for 15 minutes at room temperature was achieved with these solvents. DMSO, pyridine and 1 mol L^{-1} NH_3 lead to the best dissolution of the precipitates. Table 9 shows the experimental conditions requested to dissolve partially the precipitates in DMSO, pyridine or 1 mol L^{-1} NH_3 and the weight of the insoluble part (after the partial dissolution, a liquid phase (Φ_{F1}) and a solid ($\Phi_{S,3}$) were obtained).

Table 10 gathers palladium concentration in these solvents after partial dissolution of the precipitates $\Phi_{S,1}$ and $\Phi_{S,2}$. The accuracy on the palladium concentration and the weight percent of palladium solubilized was 5%.

$$\%_w \text{ Pd solubilized} = \frac{m_{Pd_{solubilized}}}{m_{Pd(0)}} 100 \quad (9)$$

The calculation of $m_{Pd(0)}$ is described in the TGA-DSC analysis, it corresponds to the mass remaining at 650 °C.

Equipment and analysis

ThermoGravimetric analysis coupled with a differential scanning calorimeter (TGA-DSC). Thermogravimetric analyses coupled with a differential scanning calorimeter (TGA-DSC) were performed with a LABSYS EVO model from SETARAM under nitrogen at a flow rate of 20 mL min^{-1} between 25 °C and 650 °C with a ramp of temperature of 5 °C min^{-1}. An alumina crucible (90 μL) was used as reference crucible for TGA measurements. Experiments were conducted under inert nitrogen atmosphere in order to avoid side reactions between palladium salts and dioxygen responsible for PdO formation as reported by Gallager *et al.*[67]

Table 10 Palladium concentrations and weight percent of Pd solubilized in the filtrates after partial dissolution for 15 minutes stirring of $\Phi_{S,1}$ and $\Phi_{S,2}$ in DMSO, pyridine and 1 mol L^{-1} NH_3 with a solid/liquid (S/L) ratio of 2 (mass of precipitate used for the dissolution (g)/volume of the solvent (L))

Solvents used for the dissolution	$\%_w$ Pd solubilized[a]		[Pd] solubilized (mol L^{-1})	
	$\Phi_{S,1}$	$\Phi_{S,2}$	$\Phi_{S,1}$	$\Phi_{S,2}$
DMSO	10	9	9.2×10^{-4}	1.3×10^{-3}
Pyridine	80	81	6.8×10^{-3}	1.0×10^{-2}
NH_3	99	83	9.1×10^{-3}	9.6×10^{-3}

[a] The weight percent of palladium solubilized in each solvent DMSO, pyridine and NH_3 is calculated as shown in eqn (9).

The weight loss observed around 80 °C attributed to the H_2O vaporization allows calculating the moisture content in the precipitates according to eqn (10)

$$\%\text{ Moisture} = \frac{m_{initial} - m_1}{m_{initial}} 100 \quad (10)$$

where $m_{initial}$ denotes the initial mass of the precipitate used for TGA analysis and m_1 corresponds to the remaining mass at 110 °C.

By considering that a complete degradation is achieved when the samples are heated at 650 °C, the weight percent of palladium in the precipitates can thus be calculated as follows eqn (11).

$$\%_w \text{ Pd} = \frac{m_{Pd(0)}}{m_{initial}} 100 \quad (11)$$

where $m_{Pd(0)}$ corresponds to the weight of sample at 650 °C.

The weight loss observed between 25 °C and 110 °C, from 110 °C to 350 °C, and between 350 °C and 650 °C are attributed to H_2O vaporization, organic compounds, and $(CN)_2$ respectively. The weight percent calculations are detailed below. Based on the TGA analyses, a quantification of each loss in mass can be deduced.

Table 9 Volume (V) of solvent (DMSO, pyridine or 1 mol L^{-1} NH_3) used to dissolve partially m (mg) of precipitates $\phi_{S,1}$ or $\phi_{S,2}$ and weight of insoluble fraction of solid (m′). Experimental conditions: room temperature; stirring time = 15 minutes

	Solvent								
	DMSO			Pyridine			1 mol L^{-1} NH_3		
Sample	m (mg)	V (mL)	m′ (mg)	m (mg)	V (mL)	m′ (mg)	m (mg)	V (mL)	m′ (mg)
$\Phi_{S,1}$	11.2	5.6	6.3	10.7	5.35	—[a]	11.3	5.65	0.3
$\Phi_{S,2}$	11.8	5.9	9.5	11.4	5.7	0.5	12.8	6.4	0.2

[a] m′ could not be determined since no enough insoluble fraction was obtained.

By measuring the loss in mass of $(CN)_2$ produced between 300 °C and 650 °C, TGA analysis allows the determination of the mass associated to gaseous $(CN)_2$ thanks to eqn (12).

$$m_{(CN)_2} = m_2 - m_{Pd(0)} \quad (12)$$

where $m_{(CN)_2}$ denotes the mass of $(CN)_2$ in the sample, m_2 the remaining mass of the sample at 350 °C and $m_{Pd(0)}$ the remaining mass at 650 °C.

By assuming all the $(CN)_2$ is in palladium cyanide form, it is possible to calculate the fraction of Pd linked to cyano functions present in the total amount of the Pd in the precipitate as shown in eqn (13).

$$\%_w\ Pd_{(CN)_2} = \frac{m_{(CN)_2}}{M_{(CN)_2}} M_{Pd} \frac{1}{m_{Pd(0)}} 100 \quad (13)$$

where $M_{(CN)_2}$ corresponds to the molecular weight of $(CN)_2$ and M_{Pd} denotes the molecular weight of palladium.

The weight percent of palladium linked to carboxylate present in the total amount of the Pd in the precipitate can be deduced as follows by considering that only carboxylate and CN functions are linked to palladium in the precipitates (eqn (14)).

$$\%_w\ Pd_{(O-C=O)} = 100 - \%_w\ Pd_{(CN)_2} \quad (14)$$

At 350 °C, the loss in mass is attributed to organic compounds. The weight percent of organic compound can be deduced thanks to eqn (15).

$$\%_w\ Organic = \frac{m_{initial} - m_{Pd(0)} - m_{(CN)_2} - m_{H_2O}}{m_{initial}} 100 \quad (15)$$

where $m_{initial}$ corresponds to the initial mass of the precipitate used for TGA analysis, $m_{Pd(0)}$, $m_{(CN)_2}$ and m_{H_2O} represent weight of palladium in the sample, weight of $(CN)_2$ released, and weight of water present in the sample ($m_{H_2O} = m_{initial} - m_1$), respectively.

In general, it may be considered that the TGA measurement uncertainties lead to an error of approximatively 10% for the difference weight percent calculations.

ATR-FTIR spectroscopy. IR spectra were recorded with a Fourier Transform Infrared Spectrometer Vertex 70 from BRUKER equipped with a wide range beam splitter (scan number = 32; resolution = 4 cm^{-1}) and the DTGS wide range (diamond) allowing scanning between 80 and 4000 cm^{-1}. Samples were deposited on an ATR diamond crystal.

Raman. Raman spectra were recorded with a labRAM HR evolution from HORIBA equipped with a laser with a wavelength of 633 nm. The acquisition time and the number of accumulations were of 100 seconds and 3, respectively. A quartz cell placed in the macro lens UV-Vis NIR was used. Raman spectroscopy was used to analyse the filtrate (ϕ_{F1}) obtained after a partial dissolution of the precipitate $\phi_{S,1}$ in NH_3 1 $mol.L^{-1}$ for 15 minutes of stirring at ambient temperature.

X-ray photoelectron spectroscopy. X-ray Photoelectron Spectroscopy (XPS) analyses were carried out with a ThermoFisher Escalab 250 XI spectrometer using a monochromatic Al Kα X-ray source (1486.6 eV). A dual beam charge compensation flood gun was used when important charge effects occurred and the C-1s signal for adventitious carbon was used to correct the charge effect. The C–C/C–H component of C-1s spectra was fixed at 285.0 eV. The spectrometer was calibrated to the silver Fermi level (0 eV) and to the $3d_{5/2}$ core level of metallic silver (368.3 eV). The following core levels were recorded with a 20 eV pass energy: Pd-3d, C-1s and N-1s. Data processing was performed using the commercial Avantage® software (ThermoFisher Scientific Inc.). Shirley background subtraction method was used for fitting procedure. With our results, the Pd/N ratio was calculated. The Pd/C ratio could not be calculated due to the possible presence of contaminants. An intensity ratio of the peak can be calculated supposing the atoms considered for the calculation are not pollution. This ratio is then corrected by sensitivity factors (Scofield factors have been used for quantification) and spectroscopic factors (ability of the spectrometer to detect an electron of a defined energy). Moreover, the palladium proportion of the two contributions Pd–CN and Pd–O=C–O for $\Phi_{S,1}$ and $\Phi_{S,2}$ can be calculated based on XPS analysis. By calculating the maximum intensity ratio of Pd linked to CN function and Pd linked to carboxylate function and by considering only two kinds of palladium are present in the precipitates, it is possible to obtain the palladium proportion of the two kinds of palladium. For XPS analysis, there are several sources of error in the weight percent calculated by this technique. First of all, the XPS analysis only gives information to relative quantifications. The errors can come from the choice of the background, the recombination of the spectra and a different depth of analysis from one sample to another. Finally, this technique allows analysing the extreme surface of the powder only and does not allow going deep into the sample. All this errors can explain the large uncertainty error in the value obtain by calculated of the proportions of Pd linked to cyano functions (C≡N) and Pd linked to carboxylate functions (O–C=O).

X-ray powder diffraction analysis. X-ray powder diffraction analyses (XRD) were performed by means of a D8 Advance BRUKER diffractometer equipped with a LynxEyes™ detector. A copper cathode tube was used at a voltage of 40 kV and a current of 40 mA. XRD patterns were recorded between $2\theta = 5°$ and $2\theta = 140°$ with a step of 0.01° and an acquisition time of 0.5 s per step. Powders were deposited onto a mirror sample holder (monocrystal of silicon) wetted with ethanol to paste the powders. The Diffrac software, Evaluation V2.1 and database ICDD PDF 2016 were used for indexing XRD patterns.

The precipitates were analyzed by Rietveld refinement, using TOPAS 4.2 software and Le Bail pattern matching.[81] The profile parameters (cell dimension, peak shape, background, sample displacement correction and asymmetry) were defined. The peak shape was described by pseudo-Voigt function with the formulation of Caglioti.[82]

The Rietveld method[83] was used to determine the crystallographic structure of solid samples. The refinement program minimizes the residual between experimental and calculated XRD patterns by the method of least squares. The quality of a refinement was determined by comparing the experimental XRD pattern and the calculated one by means of the following parameters, which must be as low as possible:

- The R_{Bragg} factor associated with a given structure is based on the integrated intensities and is calculated by eqn (16). The structural model is assumed to be correct when the ratio R_{Bragg} value is lower than about 5.

$$R_{Bragg} = \frac{\sum_i |I_i(obs) - I_i(calc)|}{\sum_i I_i(obs)} \quad (16)$$

where I_i(obs) and I_i(calc) denote the intensities of the peak i in the experimental and calculated XRD-pattern, respectively.

- The factor R_{wp} weighted profile is associated with the whole pattern and is calculated as follows in eqn (17):

$$R_{wp} = \sqrt{\frac{\sum_i w_i [y_i(obs) - Y_i(calc)]^2}{\sum_i w_i y_i^2(obs)}} \quad (17)$$

where y_i(obs) denotes the intensity observed to the angle $2\theta_I$, y_i(calc) corresponds to the calculated angle $2\theta_i$, and w_i denotes the statistical weight.

Electrospray-ionization mass spectroscopy. Electrospray-ionization mass spectrometry spectra (ESI-MS) were recorded in the positive ionization mode using a BRUKER Esquire-LC quadrupole ion trap equipped with an electrospray interface. A syringe infusion pump (Cole Palmer) delivered the sample at a rate of 180 μL h^{-1} to the electrospray source. The capillary voltage was set to −4000 V. Nitrogen was employed as the drying and nebulizing gas. The drying gas flow rate was set to 4.0 L min^{-1} and the nebulizing gas pressure was set to 5.0 psi. The source temperature was set to 250 °C. Spectra were acquired over a mass/charge (m/z) range of 45–2200 with a trap drive setting of 50. All samples were diluted by a factor of 10 or 100 in acetonitrile prior to any injection into the ESI-MS. Species containing Pd atom(s) were identified by comparison with an isotopic pattern calculated using the software DataAnalysis 4.0 (seen Fig. 13 as an example).

Nuclear magnetic resonance spectroscopy. Nuclear magnetic resonance spectra (^{1}H NMR) were recorded on a 400 MHz Agilent DD2 spectrometer equipped with a OneNMR probe. Solutions were diluted using deuterated dimethylsulfoxide (DMSO-D6, Aldrich) containing traces of tetramethylsilane (0.03%). The measurements were performed in a 5 mm-diameter tube. Solutions were analysed by using 1D hydrogen spectra and 2D gHSQBC and gHMBC methods.

Inductively coupled plasma – atomic emission spectroscopy. Analyses by Inductively Coupled Plasma – Atomic Emission Spectroscopy (ICP-AES) were carried out with an Ultima 2 from HORIBA. The pressure of argon and nitrogen were 6 bar and 0.5 bar, respectively. The flux of plasma-forming and sheathing gas were 12 L min^{-1} and 0.2 L min^{-1}, respectively. ICP-AES was used to measure palladium concentrations in the aqueous phases. The calibration curve was determined by using 8 standard solutions containing palladium at concentrations ranging from 0 to 20 mg L^{-1} prepared from 1 g L^{-1} commercial standard solution. The samples were diluted in 2%$_w$ nitric acid (prepared from 68.5%$_w$ nitric acid). The uncertainty obtained by ICP-MS is approximately 5%.

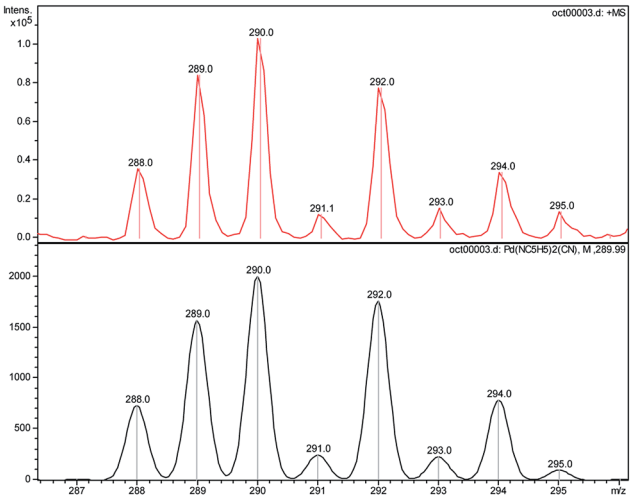

Fig. 13 Experimental (at the top) and simulated (at the bottom) isotopic pattern of $[Pd(pyr)_2(CN)]^+$.

Potentiometric titration. The acidity of the organic phases was measured by 0.04 or 0.1 mol L^{-1} NaOH standard solution (purity > 99.9% certified grade, provided by VWR) using a 785 DMP Titrino autotitrator from Metrohm. Aqueous samples were diluted in 80 mL of water (deionized water, 18.2 Ω). For organic samples analysis, samples were diluted in 80 mL of aqueous phase and 1 mL of acetone was added before titration to obtain a homogenous solution. The accuracy obtained by this method is approximately 3%.

Conflicts of interest

There are no conflicts to declare.

Acknowledgements

This research was financially supported by ORANO Cycle and Commissariat à l'Énergie Atomique et aux Énergies Alternatives (CEA). The authors would like to thanks Ashleigh Kimberlin for helpful comments and editing assistance.

References

1 H. A. C. Mc Kay, in *Science and Technology of Tributyl Phosphate*, ed. W.W. Schulz and James D. Navratil, CRC Press, Boca Raton, Florida, 1984, vol. 1, pp. 1–12.
2 R. Ruhela, A. K. Singh, B. S. Tomar and R. C. Hubli, *RSC Adv.*, 2014, **4**, 24344.
3 M. C. Charbonnel and L. Berthon, in *Ion Exchange and Solvent Extraction*, ed. B. Moyer, CRC Press Taylor & Francis Group, Boca Raton, London, New York, 2010, vol. 19, pp. 429–513.
4 J. W. Davis, in *Science and Technology of Tributyl Phosphate*, ed. W.W. Schulz and James D. Navratil James, CRC Press, Boca Raton, Florida, 1984, vol. 1, pp. 221–266.

5 G. S. Barney and D. G. Bouse, *Alpha radiolysis of tributyl phosphate – Effect of diluents*, Atlantic Richfield Hanford Company, ARH-ST-153, Washington, 1977.
6 I. A. Kulikov, N. V. Kermanova, O. A. Sosnovskii, N. N. Shesterikov and M. V. Vladimirova, *Sov. Radiochem.*, 1981, **23**, 664–669.
7 Y. Gao, W. Zheng, X. Cao and S. Chen, *Nukleonika*, 2014, **59**, 123–128.
8 J. Pearson and M. Nilsson, *Solvent Extr. Ion Exch.*, 2014, **32**, 584–600.
9 I. A. Kulikov, N. V. Kermanova and M. V. Vladimirova, *Sov. Radiochem.*, 1983, **25**, 310–316.
10 V. M. Adamov and V. I. Andrew, *Kerntechnik*, 1990, **55**, 133–136.
11 Z. Nowak, *Nukleonika*, 1977, **22**, 155–172.
12 E. Vialard and M. Germain, in *Extraction 84: Symposium on Liquid-Liquid Extraction*, ed. Yong Zhou, Pergamon Press, Dounreay (UK), 1984, vol. 88, pp. 19–30.
13 E. S. Lane, *Nucl. Sci. Eng.*, 1963, **17**, 620–625.
14 O. K. Tallent, J. C. Mailen and K. D. Pannel, *Nucl. Technol.*, 1985, **2**, 417–425.
15 G. F. Egorov and O. P. Afanas'ev, *At. Energy*, 1983, **54**, 347–355.
16 S. C. Tripathi, P. Bindu and A. Ramanujam, *Sep. Sci. Technol.*, 2001, **36**, 1463–1478.
17 B. J. Mincher, S. P. Mezyk and L. R. Martin, *J. Phys. Chem.*, 2008, **112**, 6275–6280.
18 S. Mishra, C. Mallika, N. K. Pandey, U. Kamachi Mudali and R. Natarajan, *Sep. Sci. Technol.*, 2015, **50**, 1671–1676.
19 Z. Nowak, M. Nowak and A. Seydel, *Radiochem. Radioanal. Lett.*, 1979, **38**(5–6), 343–354.
20 V. M. Adamov, V. I. Andreev, B. N. Belyaev, G. S. Markov, M. S. Polyakov, A. E. Ritori and A. Y. Yu Shil'nikov, *Sov. Radiochem.*, 1991, **24**, 153–158.
21 M. V. Krishnamurthy and R. Sampathkumar, *J. Radioanal. Nucl. Chem. Lett.*, 1992, **166**(5), 421–429.
22 Z. Nowak and M. Nowak, *Radiochem. Radioanal. Lett.*, 1973, **14**(3), 161–168.
23 D. Lesage, PhD thèse, Université de Paris VI, 1995.
24 D. Lesage, H. Virelizier, C. K. Jankowski and J. C. Tabet, *J. Spectrosc.*, 1997, **13**, 275–290.
25 D. Lesage, H. Virelizier, C. K. Jankowski and J. C. Tabet, *Eur. Mass Spectrom.*, 1998, **4**, 47–54.
26 M.-C. Charbonnel and L. Berthon, *Ion Exch. Solvent Extr.*, 2009, **19**, 17–24.
27 B. J. Mincher, G. Modolo and S. P. Mezyk, *Solvent Extr. Ion Exch.*, 2009, **27**, 1–25.
28 V. Huss, PhD thesis, University of Aix-Marseille, 1991.
29 S. C. Tripathi and A. Ramanujam, *Sep. Sci. Technol.*, 2003, **38**, 2307–2326.
30 C. J. Hardy and D. Scargill, *J. Inorg. Nucl. Chem.*, 1961, **17**, 337–349.
31 J. C. Neace, *Sep. Sci. Technol.*, 1983, **18**, 1581–1594.
32 C. Miyake, M. Hirose, T. Yoshimura, M. Ikeda, S. Imoto and M. Sano, *J. Nucl. Sci. Technol.*, 1990, **27**, 157–166.
33 D. N. Smith, H. G. M. Edwards, M. A. Hughes and B. Courtney, *Sep. Sci. Technol.*, 1997, **32**, 2821–2849.
34 E. Zimmer and J. Bochardt, *Nucl. Technol.*, 1986, **75**, 332–337.
35 C. Miyake, M. Hirose, T. Yoshimura, M. Ikeda, S. Imoto and M. Sano, *J. Nucl. Sci. Technol.*, 1990, **27**, 256–261.
36 K. P. Lunichkina, E. V. Renard and V. B. Shevchenko, *Russ. J. Inorg. Chem.*, 1974, **19**, 110–113.
37 H. X. Huang, G. H. Zhu and S. B. Hou, *Radiochim. Acta*, 1989, **46**, 159–162.
38 S. Tachimori, H. Nakamura and A. Sato, *J. Radioanal. Nucl. Chem.*, 1979, **50**, 143–151.
39 B. A. Powell, J. D. Navratil and M. C. Thompson, *Solvent Extr. Ion Exch.*, 2003, **21**, 347–368.
40 P. A. Zagorets, *Sov. Radiochem.*, 1982, **24**, 43–48.
41 L. L. Burger, in *Progress in Nuclear Energy*, ed. F. R. Bruce, J. M. Fletcher and H. H. Hyman, Pergamon Press, New York, 1958, vol. 2, p. 307.
42 M. V. Vladimirova, D. A. Fedoseev, I. A. Kulikov, I. A. Boikova, A. S. Milovanova and N. V. Kermanova, *Sov. Radiochem.*, 1984, **26**, 84–89.
43 M. V. Vladimirova, D. A. Fedoseev, I. A. Kulikov, A. S. Milovanova, I. A. Boikova, O. A. Sosnovskii, N. V. Kermanova and B. I. Bulkin, *Sov. Radiochem.*, 1981, **24**, 33–38.
44 M. V. Vladimirova, D. A. Fedoseev, I. A. Boikova and A. S. Milovanova, *Sov. Radiochem.*, 1984, **26**, 29–36.
45 L. P. Sokina, A. S. Solovkin, E. G. Teterin, F. A. Bogdanov and N. N. Shesterikov, *Sov. Radiochem.*, 1978, **20**, 19–24.
46 P. Zhang, C. L. Song, J. F. Liang and R. X. Xin, *Solvent Extr. Ion Exch.*, 2001, **19**, 79–89.
47 C. A. Blake Jr, W. Davis Jr and J. M. Schmitt, *Nucl. Sci. Eng.*, 1963, **17**, 626–637.
48 A. M. Rochon, Z. Nowak and Z. P. Zagorski, *Radiochem. Radioanal. Lett.*, 1976, **27**, 1–8.
49 C. Lamouroux, C. Moulin, J. C. Tabet and C. K. Jankowki, *Rapid Commun. Mass Spectrom.*, 2000, **14**, 1869–1877.
50 E. V. Barelko, I. P. Solyanina and G. S. Babakina, *Sov. Radiochem.*, 1976, **18**, 573–577.
51 E. G. Teterin, N. N. Shesterikov, P. G. Krutikov and A. S. Solovkin, *Russ. J. Inorg. Chem.*, 1971, **16**, 77–80.
52 N. Uetake, *J. Nucl. Sci. Technol.*, 1989, **26**, 329–338.
53 J. H. Mesisenhelder and A. A. Siczek, *Radiochim. Acta*, 1980, **27**, 223–227.
54 H. G. M. Edwards, M. A. Hughes, D. N. Smith and B. Courtney, *J. Mol. Struct.*, 1995, **351**, 65–76.
55 H. Sugai and K. Munakata, *Nucl. Technol.*, 1992, **99**, 235–241.
56 G. Modolo and S. Seekamp, *Solvent Extr. Ion Exch.*, 2002, **20**, 195–210.
57 B. Weaver and F. A. Kappelmann, *J. Inorg. Nucl. Chem.*, 1968, **30**, 263–272.
58 V. Guedon, PhD thèse, Université de Grenoble I, 1993.
59 V. Guedon, J. C. Thieblemont, Y. Revel and A. Vandrot, *J. Nucl. Sci. Technol.*, 1994, **31**, 48–61.
60 J. Ly, PhD thèse, Université de Paris VI, 1984.
61 E. V. Renard, *Sov. Radiochem.*, 1976, **18**, 560–571.
62 S. De Sio, I. Klur, E. Tison, C. Bouyer, D. Lebeau, F. Goutelard, L. Séjourné, C. Eysseric and N. Vigier, *Procedia Chem.*, 2016, **21**, 17–23.

63 S. J. Hibble, A. M. Chippindale, E. J. Bilbé, E. Marelli, P. J. F. Harris and A. C. Hannon, *Inorg. Chem.*, 2011, **50**, 104–113.
64 G. Beamson and D. Briggs, *High Resolution XPS of Organic Polymers: the Scienta Esca 300 Database*, John Wiley and Sons Ltd, UK, 1992.
65 L. Soptrajanova and B. Soptrajanov, *Spectrosc. Lett.*, 1992, **25**, 1131–1139.
66 B. Bulkin and R. Rose, *Appl. Spectrosc.*, 1978, **32**, 151–157.
67 P. K. Gallagher and M. E. Gross, *J. Therm. Anal.*, 1986, **31**, 1231–1241.
68 L. Huang, Y. Wang, Z. Wang and F. Chen, *Physical Chemistry*, 2012, **2**, 27–34.
69 A. G. Sharpe, in *The Chemistry of Cyano Complexes of the Transition Metals*, Academic Press, London, New York, 1976, vol. 11, pp. 243–248.
70 F. P. Miner, A. R. Kajanjian, A. K. Brown, P. G. Hagan and J. W. Berry, *Radiation chemistry of nitric acid solutions – Technical Report RFP–1299*, 1969.
71 A. J. Huggard and B. F. Warner, *Nucl. Sci. Eng.*, 1963, **17**, 638–650.
72 A. Dakshinamoorthy, P. S. Dhami, P. W. Naik, N. L. Dudwadkar, S. K. Munshi, P. K. Dey and V. Venugopal, *Desalination*, 2008, **232**, 26–36.
73 N. Getoff, *Radiat. Phys. Chem.*, 2006, **75**, 514–523.
74 V. M. Adamov, *Radiokhimia*, 1987, **29**, 822–829.
75 Y. Tashiro, R. Kodama, H. Sugai, K. Suzuki and S. Matsuoka, *Nucl. Technol.*, 2000, **129**, 93–100.
76 J. Kuruc, A. Petrů, R. Čech and P. Rajec, *J. Radioanal. Nucl. Chem.*, 1996, **208**, 351–368.
77 H. Modler and M. Nonomura, *Toxicol. Environ. Chem.*, 1995, **48**, 155–175.
78 A. Costagliola, L. Venault, A. Deroche, G. Garaix, J. Vermeulen, R. Omnee, F. Duval, G. Blain, J. Vandenborre, M. Fattahi-Vanani and N. Vigier, *Radiat. Phys. Chem.*, 2016, **119**, 186–193.
79 B. Braithwate, *Chem. Commun.*, 1969, **22**, 1329.
80 J. M. Harrington, S. B. Jones and R. D. Hancock, *Inorg. Chim. Acta*, 2005, **358**, 4473–4480.
81 AXS BRUKER, *Software TOPAS – version 4.2*, 2009.
82 G. Caglioti, A. Paelotti and F. P. Ricci, *Nucl. Instrum.*, 1958, **3**, 223–228.
83 H. Rietveld, *J. Appl. Crystallogr.*, 1969, **2**, 65–71.